Rock and Soil Mechanics

Volume 42 | Issue 5 Article 2

9-16-2021

# Rock plastic-damage constitutive model based on energy dissipation

Qiu-feng MA
*School of Resources and Environmental Engineering, Shandong University of Technology, Zibo, Shandong 255000, China*

Zhi-he LIU
*School of Resources and Environmental Engineering, Shandong University of Technology, Zibo, Shandong 255000, China*

Yue-ping QIN
*School of Emergency Management and Safety Engineering, China University of Mining and Technology (Beijing), Beijing 100083, China*

Jing TIAN
*Department of Mechanical Engineering, Zikuang University, 255120, Zibo, Shandong 255120, China*

*See next page for additional authors*



## Custom Citation

MA Qiu-feng, LIU Zhi-he, QIN Yue-ping, TIAN Jing, WANG Shu-li, . Rock plastic-damage constitutive model based on energy dissipation[J]. Rock and Soil Mechanics, 2021, 42(5): 1210-1220.

# Rock plastic-damage constitutive model based on energy dissipation


## Authors

Qiu-feng MA, Zhi-he LIU, Yue-ping QIN, Jing TIAN, and Shu-li WANG

Rock and Soil Mechanics 2021 42(5): 1210−1220 ISSN 1000−7598
https: //doi.org/10.16285/j.rsm.2020.6091 rocksoilmech.researchcommons.org/journal

# Rock plastic-damage constitutive model based on energy dissipation

MA Qiu-feng[1], LIU Zhi-he[1], QIN Yue-ping[2], TIAN Jing[3], WANG Shu-li[1]

1. School of Resources and Environmental Engineering, Shandong University of Technology, Zibo, Shandong 255000, China
2. School of Emergency Management and Safety Engineering, China University of Mining and Technology (Beijing), Beijing 100083, China
3. Department of Mechanical Engineering, Zikuang University, 255120, Zibo, Shandong 255120, China

**Abstract:** In this paper, the dissipative energy in the damage process was employed to solve the damage variable while the damage constitutive model was established. In this model, the Mohr-Coulomb criterion and the energy dissipation theory were introduced. Considering the hardening and softening characteristics of rock during loading, the non-associated plastic flow rule was applied to describe the plastic deformation of rock, and the damage variable was calculated by quoting the dissipation energy and damage energy dissipation rate in the damage process. Based on the conventional triaxial loading-unloading experiments, the energy consumption and damage evolution law of rock was analyzed. The expression of damage energy dissipation rate was established, and the parameters in the model were calibrated. Simulation was conducted by this model and the simulation results were compared with the experimental results to validate the model. In this process, the following conclusions were obtained: (1) in the elastic stage, the damage dissipation energy increases slowly with the axial strain, showing an upward concave curve, and the growth rate reaches the maximum near the peak-stress. In the residual stage, the relationship between damage dissipation energy and axial strain is linear; (2) based on elastic modulus associated damage definition, the experimental results show that there is a damage variable limit less than 1, and the damage variable limit gradually decreases with the increase of confining pressure; (3) the model in this paper can be used to investigate the strength, hardening, softening characteristics and strain law of rock under different confining pressures during the loading process. The numerical simulation results can describe the stress-strain relationship and damage evolution law of rock.

**Keywords:** damage; energy dissipation; Mohr-Coulomb criterion; constitutive model; damage energy consumption rate

## 1 Introduction

In recent years, the development of damage mechanics has provided an effective method for the analysis of the mechanical properties of rock material. According to the law of thermodynamics, energy conversion is the essential feature of the physical process of matter, and the rock must dissipate energy during the damage process[1]. Using the dissipated energy in the damage process to solve the damage variables, and then to establish a damage constitutive model, will become a new modeling method. A large number of scholars have studied the law of energy dissipation during rock loading–unloading. Han et al.[2], Qin et al.[3], Xu et al.[4], Li et al.[5], Zhang et al.[6] and others conducted mechanical tests on the rock, and analyzed the elastic strain energy accumulated during the test and the energy dissipation. They deemed the changing law of energy dissipation is that the dissipation ratio presents a trend of increasing–decreasing–increasing. Xie et al.[7–8] defined criteria for rock strength failure and criteria for overall failure of rock mass based on the principle of energy dissipation and release. Jiang et al.[9] conducted triaxial tests on mudstones in dry, natural and saturated states, and explored the influence of water content on rock mechanical properties and energy evolution. Yang et al.[10], Cong et al.[11], Li et al.[12] performed loading–unloading tests on granite and other rocks, analyzed the effects of different loading rates on the elastic strain energy and damage dissipation energy in the rock, and also analyzed the transformation relationship between different types of energy. Zhao et al.[13] carried out comparative tests on sandstones in northeastern and western China, and investigated the characteristics of energy dissipation. Qiao et al.[14] designed a shear friction test and determined the friction dissipation energy under different vertical stress levels by calculating the area under the shear stress–strain curve. Yin et al.[15] used self-developed true triaxial test apparatus to carry out loading–unloading mechanical tests on sandstone, and analyzed the influence of different loading rates on the energy evolution law.

At present, we have a basic understanding of the energy conversion law of rocks during loading, and many damage models have been developed to describe the mechanical properties of rocks. Based on the test results, Peng et al.[16] established a damage evolution model for coal stiffness degradation before peak strength, and used it to determine the initial damage and critical damage variables. He et al.[17] conducted fatigue tests on rock salt under different stress amplitudes, loading frequencies, confining pressures and loading rates, and established a cumulative dissipation energy evolution model. Based on the principle of energy dissipation, Ning et al.[18] developed a new method for identifying the threshold

Received: 27 July 2020 Revised: 6 January 2021
This work was supported by the Youth Foundation of National Natural Science Foundation of China (51904177) and the National Natural Science Foundation of China (50904071).
First author: MA Qiu-feng, male, born in 1990, PhD candidate, Lecturer, mainly engaged in research on rock mechanics and numerical calculation. E-mail: maqiufeng666@sina.com

of crack initiation and propagation. Liu et al.[19] defined the damage variable with energy dissipation as the bridge, and gave the damage evolution equation of the rock under cyclic loading and unloading conditions. Xie et al.[7] analyzed the critical stress of the overall failure of the rock element under various stress states, and used this criterion to discuss the critical conditions for the failure of the tunnel surrounding rock.

Based on the existing research work, the expressions of damage variables are fitted under given test conditions, and the expressions can only be applied to the damage evolution law under test conditions. The damage evolution law under complex loading conditions needs to be further improved. This paper aims to establish a damage variable solution method, that is, the damage variable is obtained by dividing the damage dissipated energy by the damage energy consumption rate, and then the damage constitutive model is established to describe the mechanical properties of the rock in the damage process.

## 2 Basic model equations

### 2.1 Stress-strain relationship

2.1.1 Definition of damage variables

In this paper, the damage variable is defined in the form of scalar, and the loss of stiffness during the damage process is used to describe the magnitude of the damage variable. This method is the most widely used damage variable definition method at present, and its expression is

$$D = 1 - \frac{E}{E_0} \tag{1}$$

where $D$ is the damage variable; $E$ is the elastic modulus in the damaged state; $E_0$ is the elastic modulus in the undamaged state, which is referred to as the initial elastic modulus for short. Based on the above definition method, the elastic modulus in the damaged state can be written as

$$E = E_0(1-D) \tag{2}$$

2.1.2 Strain hypothesis

Assuming that the strain consists of two parts: elastic strain and plastic strain, the expression of strain

$$\boldsymbol{\varepsilon} = \boldsymbol{\varepsilon}^{\mathrm{e}} + \boldsymbol{\varepsilon}^{\mathrm{p}} \tag{3}$$

where $\boldsymbol{\varepsilon}$ is the strain tensor; $\boldsymbol{\varepsilon}^{\mathrm{e}}$ is the elastic strain tensor; and $\boldsymbol{\varepsilon}^{\mathrm{p}}$ is the plastic strain tensor.

The prescribed stress and strain tensors are expressed in the form of 6 components, and their orders are arranged in the *xx*, *yy*, *zz*, *xy*, *xz*, and *yz* directions, which will not be described in the following. For example, the component expression of the elastic strain tensor is

$$\boldsymbol{\varepsilon}^{\mathrm{e}} = \left(\varepsilon_{xx}^{\mathrm{e}}, \varepsilon_{yy}^{\mathrm{e}}, \varepsilon_{zz}^{\mathrm{e}}, \varepsilon_{xy}^{\mathrm{e}}, \varepsilon_{xz}^{\mathrm{e}}, \varepsilon_{yz}^{\mathrm{e}}\right)^{\mathrm{T}} \tag{4}$$

where $(\cdot)^{\mathrm{T}}$ means transpose.

2.1.3 Stress–strain relationship equations

According to Hooke's law, the stress–strain relationship of a rock can be written as

$$\boldsymbol{\sigma} = (1-D)\boldsymbol{M}_0\boldsymbol{\varepsilon}^{\mathrm{e}} \tag{5}$$

where $\boldsymbol{\sigma}$ is the stress tensor; and $\boldsymbol{M}_0$ is the stiffness matrix in the undamaged state, and its expression is

$$\boldsymbol{M}_0 = \frac{E_0(1-\mu)}{(1+\mu)(1-2\mu)} \cdot \begin{bmatrix} 1 & \frac{\mu}{1-\mu} & \frac{\mu}{1-\mu} & 0 & 0 & 0 \\ & 1 & \frac{\mu}{1-\mu} & 0 & 0 & 0 \\ & & 1 & 0 & 0 & 0 \\ & & & \frac{1-2\mu}{1-\mu} & 0 & 0 \\ & \text{Sym} & & & \frac{1-2\mu}{1-\mu} & 0 \\ & & & & & \frac{1-2\mu}{1-\mu} \end{bmatrix} \tag{6}$$

where $\mu$ is the Poisson's ratio. Therefore, the stress increment expression is

$$\mathrm{d}\boldsymbol{\sigma} = (1-D)\boldsymbol{M}_0\mathrm{d}\boldsymbol{\varepsilon} - (1-D)\boldsymbol{M}_0\mathrm{d}\boldsymbol{\varepsilon}^{\mathrm{p}} - \boldsymbol{M}_0\boldsymbol{\varepsilon}^{\mathrm{e}}\mathrm{d}D \tag{7}$$

where $\mathrm{d}\boldsymbol{\varepsilon}$ is the strain increment; $\mathrm{d}\boldsymbol{\varepsilon}^{\mathrm{p}}$ is the plastic strain increment; and $\mathrm{d}D$ is the damage variable increment.

### 2.2 Plastic flow rule

For rock-like materials, the non-associative flow rule is usually used, and the plastic strain increment is obtained by the plastic potential function $G$, and its expression is

$$\mathrm{d}\boldsymbol{\varepsilon}^{\mathrm{p}} = \mathrm{d}\lambda\frac{\partial G}{\partial \boldsymbol{\sigma}} \tag{8}$$

where $\mathrm{d}\lambda$ is the plasticity factor, the occurrence of plastic flow is determined by the loading conditions, and its expression is [20]

$$f(\boldsymbol{\sigma}, \varepsilon^{\mathrm{ps}}, D) \leqslant 0,\ \ \mathrm{d}\lambda \geqslant 0,\ \ f(\boldsymbol{\sigma}, \varepsilon^{\mathrm{ps}}, D)\mathrm{d}\lambda = 0 \tag{9}$$

where $f(\boldsymbol{\sigma}, \varepsilon^{\mathrm{ps}}, D)$ is the plastic yield function; and $\varepsilon^{\mathrm{ps}}$ is the equivalent plastic strain. In the process of plastic flow, the incremental expression form is

$$\mathrm{d}f = f^{\boldsymbol{\sigma}}\mathrm{d}\boldsymbol{\sigma} + f^{\varepsilon^{\mathrm{p}}}\mathrm{d}\varepsilon^{\mathrm{ps}} + f^{\mathrm{D}}\mathrm{d}D \tag{10}$$

where $f^{\boldsymbol{\sigma}} = \dfrac{\partial f}{\partial \boldsymbol{\sigma}}$, $f^{\varepsilon^{\mathrm{ps}}} = \dfrac{\partial f}{\partial \varepsilon^{\mathrm{ps}}}$, $f^{\mathrm{D}} = \dfrac{\partial f}{\partial D}$。

### 2.3 Energy conservation law formula

If a unit volume of rock produces a certain amount of deformation in the process of external force loading, we assume that the rock is in a closed system and there is no heat exchange with the outside world. According to the law of conservation of energy, the work done by the external force on the rock, the elastic strain energy of the rock, and the energy dissipated by damage satisfies the law of conservation of energy, and the formula is as follows:

$$U = U^{\mathrm{d}} + U^{\mathrm{e}} \tag{11}$$

where $U$ is the work done by the outside world to the closed system; $U^{\mathrm{d}}$ is the dissipated energy of unit rock, which is used to form internal rock damage and plastic deformation; and $U^{\mathrm{e}}$ is the elastic strain energy (set the initial elastic strain energy to 0).

The work done by the external force on the rock per unit volume can be obtained by the following integral formula:

$$U=\int(\boldsymbol{\sigma})^{\mathrm{T}}\,\mathrm{d}\boldsymbol{\varepsilon} \tag{12}$$

After the elastic strain tensor and stiffness matrix are known, the expression of elastic strain energy is

$$U^{\mathrm{e}}=\frac{1}{2}\left(\boldsymbol{\varepsilon}^{\mathrm{e}}\right)^{\mathrm{T}}\boldsymbol{M}\boldsymbol{\varepsilon}^{\mathrm{e}} \tag{13}$$

where $\boldsymbol{M}$ is the stiffness matrix after damage, $\boldsymbol{M}=(1-D)\boldsymbol{M}_0$

For any micro-element process, the incremental form of elastic strain is

$$\mathrm{d}U^{\mathrm{e}}=\frac{1}{2}\left(\mathrm{d}\boldsymbol{\varepsilon}^{\mathrm{e}}\right)^{\mathrm{T}}\boldsymbol{M}\boldsymbol{\varepsilon}^{\mathrm{e}}-\frac{1}{2}\left(\boldsymbol{\varepsilon}^{\mathrm{e}}\right)^{\mathrm{T}}\boldsymbol{M}_0\boldsymbol{\varepsilon}^{\mathrm{e}}\mathrm{d}D+\frac{1}{2}\left(\boldsymbol{\varepsilon}^{\mathrm{e}}\right)^{\mathrm{T}}\boldsymbol{M}\mathrm{d}\boldsymbol{\varepsilon}^{\mathrm{e}}=\left(\boldsymbol{\varepsilon}^{\mathrm{e}}\right)^{\mathrm{T}}\boldsymbol{M}\mathrm{d}\boldsymbol{\varepsilon}^{\mathrm{e}}-\frac{1}{2}\boldsymbol{\varepsilon}^{\mathrm{e}}\boldsymbol{M}_0\boldsymbol{\varepsilon}^{\mathrm{e}}\mathrm{d}D \tag{14}$$

Due to symmetry, the term $\frac{1}{2}\left(\mathrm{d}\boldsymbol{\varepsilon}^{\mathrm{e}}\right)^{\mathrm{T}}\boldsymbol{M}\boldsymbol{\varepsilon}^{\mathrm{e}}$ in Eq.(14) is equal to $\frac{1}{2}\left(\boldsymbol{\varepsilon}^{\mathrm{e}}\right)^{\mathrm{T}}\boldsymbol{M}\mathrm{d}\boldsymbol{\varepsilon}^{\mathrm{e}}$, so they are combined into one term.

Here, $Y$ is defined as the energy dissipated per unit damage, which is called the damage energy consumption rate. The method of dividing the damage dissipation energy $\mathrm{d}U^{\mathrm{d}}$ by the damage energy consumption rate $Y$ is used to solve the damage variable increment $\mathrm{d}D$, which is the incremental form of the damage variable. The definition formula of the damage variable is shown in equation (1). According to this, the increase of the dissipated energy $\mathrm{d}U^{\mathrm{d}}$ can be calculated by the product of damage variable increment $\mathrm{d}D$ and damage energy consumption rate $Y$, the expression is

$$\mathrm{d}D=\frac{\mathrm{d}U^{\mathrm{d}}}{Y},\ \mathrm{d}U^{\mathrm{d}}=Y\mathrm{d}D \tag{15}$$

According to the second law of thermodynamics $\mathrm{d}U^{\mathrm{d}}\geqslant 0$, $Y\geqslant 0$, $\mathrm{d}D\geqslant 0$,

For any infinitesimal process, the incremental form of the law of conservation of energy is

$$\mathrm{d}U=\mathrm{d}U^{\mathrm{e}}+\mathrm{d}U^{\mathrm{d}} \tag{16}$$

Substituting the differential form of Eq.(12) and the second term in Eqs. (14) and (15) into Eq. (16), we can get

$$(\boldsymbol{\sigma})^{\mathrm{T}}\mathrm{d}\boldsymbol{\varepsilon}=\left(\boldsymbol{\varepsilon}^{\mathrm{e}}\right)^{\mathrm{T}}\boldsymbol{M}\left(\mathrm{d}\boldsymbol{\varepsilon}-\mathrm{d}\lambda\frac{\partial G}{\partial\boldsymbol{\sigma}}\right)-\frac{1}{2}\left(\boldsymbol{\varepsilon}^{\mathrm{e}}\right)^{\mathrm{T}}\boldsymbol{M}_0\boldsymbol{\varepsilon}^{\mathrm{e}}\mathrm{d}D+Y\mathrm{d}D \tag{17}$$

So far, Eq. (10) is derived from the plastic yield function and Eq. (17) is derived from the formula of the law of conservation of energy. Both formulas contain two unknown quantities of plastic factor $\mathrm{d}\lambda$ and damage variable increment $\mathrm{d}D$, and these two unknowns can be calculated simultaneously by solving the two equations (Eqs. (10) and (17)).

## 3 Plasticity-damage model building

### 3 Determination of damage energy consumption rate formula

3.1.1 Method for measuring elastic modulus

The laboratory results show that the stress–strain curve of the rock has non-linear deformation characteristics to a certain extent during the unloading process. Even for hard granite, marble, etc., their stress–strain curves are not absolute straight lines in appearance. This brings certain difficulties to determining the elastic modulus during rock unloading.

The elastic strain energy stored in the rock is an important indicator for analyzing dynamic disaster accidents. Therefore, an approach from the perspective of elastic strain energy is developed to determine the elastic modulus of the rock during unloading. The elastic modulus obtained by this method in this paper is consistent with that measured in the experiment when calculating elastic strain energy. The specific procedure is as follows:

Figure 1 shows the stress–strain curve of sandstone during loading–unloading under the condition of 10 MPa. The loading curve is displayed as *OAB* in the figure. When loaded to point *B*, unloading starts, and the actual unloading curve is *BCF* in the figure. At point *B*, the elastic strain energy stored in the rock in the axial direction can be calculated from the elastic strain energy released by the rock during the unloading process, expressed by the area enclosed by the unloading curve and the strain axis (the area enclosed by the *FCBKF* in the figure).

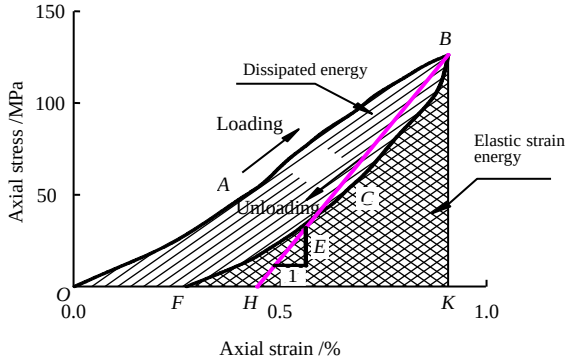


**Fig. 1 Measurement method of elastic modulus**

Suppose there is a straight line passing through point *B*, as shown by the line *BH* in the figure. The straight line satisfies the following characteristics: the area surrounded by the straight line *BH* and the strain axis equals the area enclosed by the unloading curve and the strain axis. That is, the elastic strain energy released by unloading along the straight line *BH* is equal

to the elastic strain energy released along the actual unloading curve *BCF*. At this moment, it is assumed that the elastic modulus *E* shown by the straight line *BH* is the elastic modulus of the rock at the moment of unloading. Meanwhile, it is assumed that the line segment *HK* is the elastic strain $\varepsilon_1^{\mathrm{e}}$ before unloading, and the line segment *OH* is the plastic strain $\varepsilon_1^{\mathrm{p}}$ of the rock.

3.1.2 Determination of damage energy consumption rate during the test

Based on the above-mentioned elastic modulus damage variable definition method, the conventional triaxial loading–unloading test is used to determine the damage energy consumption rate. The sandstone used in test is sampled from the Zigong area of Sichuan province. After measurements, the average density of sandstone is 2.46 g/cm$^3$. Sandstone is made into a cylinder with a diameter of 50 mm and a height of 100 mm, as shown in Fig. 2(a). We design 5 groups of different confining pressures: 0, 5, 10, 20, and 30 MPa. The RLJW-2000 electro-hydraulic servo rock triaxial compression testing machine is used to carry out the conventional loading–unloading triaxial compression test. The test press and gripper are shown in Figs. 2(b) and 2(c). After loading–unloading is completed, the fracture morphology of the rock is shown in Fig. 2(d) (confining pressure is 10 MPa). One-way continuous loading test were also carried out to determine the material parameters besides the cyclic loading and unloading tests.

The loading process is as follows. Firstly, apply confining pressure to the set confining pressure value, then stop the confining pressure loading, at this moment, the axial displacement is cleared. Then load (or unload) the specimen at a uniform speed at an axial loading rate of 0.005 mm/s. In the process of loading–unloading, the loading is performed again after unloading is conducted to the axial stress being zero. During the test, data was collected every 0.2 s.

(a) Rock samples and groups

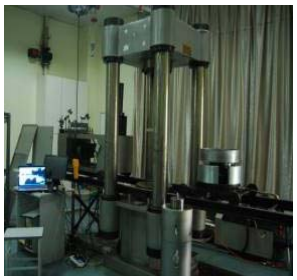

(b) Servo press

(c) Gripper and radial displacement monitoring

(d) Rock fracture pattern

**Fig. 2 Experimental equipment and materials**

The stress–strain curves during the loading and unloading test are shown in Fig. 3. In the figure, the abscissa represents the axial strain $\varepsilon_1$, and the ordinate represents the axial stress $\sigma_1$. Figures 3 (a)–(e) show the test results of the confining pressures of 0, 5, 10, 20, and 30 MPa, respectively.

Using the test results in Fig. 3, the dissipated energy during the cyclic loading–unloading process is calculated. The calculation method and results are shown in Fig. 4. In the figure, the 9th cycle under the condition of a confining pressure of 5 MPa is analyzed as an example. In the 9th cycle, the increment in damage dissipation energy $\mathrm{d}U_9^{\mathrm{d}}$ is expressed as

$$U_9^{\mathrm{d}} = \int \sigma_1^{\mathrm{load}} \mathrm{d}\varepsilon + 2\sigma_3 \Delta\varepsilon_3 - \int \sigma_1^{\mathrm{unload}} \mathrm{d}\varepsilon + 2\sigma_3 \Delta\varepsilon_3' \tag{18}$$

where $\int \sigma_1^{\mathrm{load}} \mathrm{d}\varepsilon + 2\sigma_3 \Delta\varepsilon_3$ represents the work density done by the external force on the specimen during the cycle, as presented in the upper right corner of Fig. 4; the area enclosed by the axial stress–strain curve in the loading phase in the 9th cycle is the value of the integral term. $\int \sigma_1^{\mathrm{unload}} \mathrm{d}\varepsilon + 2\sigma_3 \Delta\varepsilon_3'$ represents the elastic strain energy released by the cycle. As shown in the small graph at the lower right of Fig. 4, the area surrounded by the axial stress–strain curve in the unloading phase is the value of the integral term. Where $\sigma_1^{\mathrm{load}}$ is the axial stress during the loading process; $\sigma_1^{\mathrm{unload}}$ is the axial stress during the unloading process; $\Delta\varepsilon_3$ is the increment in the radial strain during the loading process; $\Delta\varepsilon_3'$ is the increment in the radial strain during the unloading process.

Finally, the increment in damage dissipation energy during each cycle is determined by the above formula. To obtain the dissipated energy–axial strain relationship diagram, we accumulate the dissipated energy of each cycle as shown in Fig. 4.

Using the test results in Fig. 3, the damage variables during the cycle loading–unloading process are calculated. The calculation method and calculation results are shown in Fig. 5(a). Figure 5(b) takes the 14th cycle of 30 MPa as an example, and the formula for solving the damage variable is

$$D_{14} = 1 - \frac{E_{14}}{E_0} \tag{19}$$

where $E_{14}$ is the elastic modulus during the 14th cycle of unloading, and the method in Fig. 1 is used to determine the elastic modulus.

The value of the damage variable can be obtained through the above calculation method, and the damage variable is drawn to obtain the damage variable–axial strain relationship diagram, as shown in Fig. 5.

It can be observed from Fig. 4 that the magnitude of the dissipated energy under different confining pressures has a significant difference, the greater the confining pressure, the greater the damage dissipated energy.

Although there are differences in numerical values, the law of change is consistent. When the strain is less than 1%, the damage dissipated energy increases slowly with the axial strain, showing an upward concave curve,

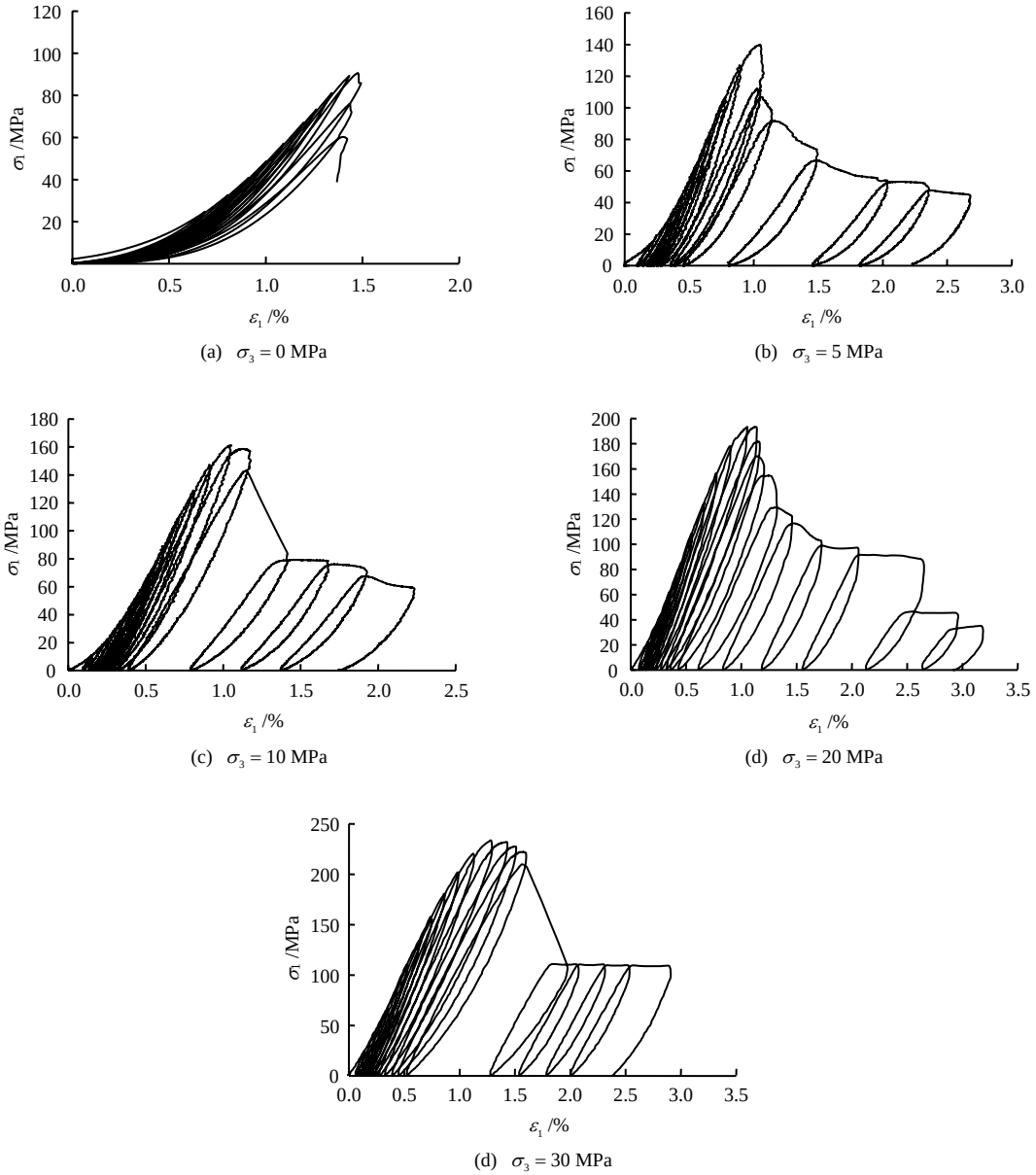


**Fig. 3 Stress–strain relationships of loading–unloading experiments**

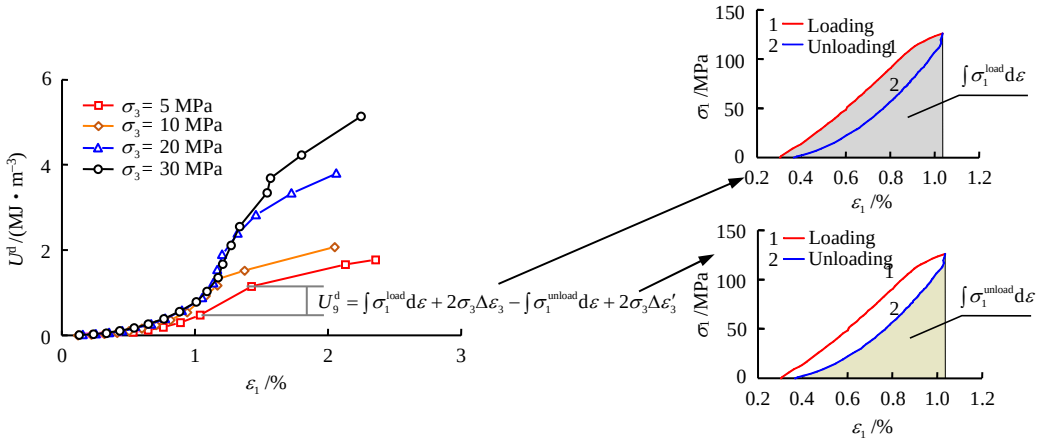


**Fig. 4 Relationships between damage dissipated energy and axial strain**

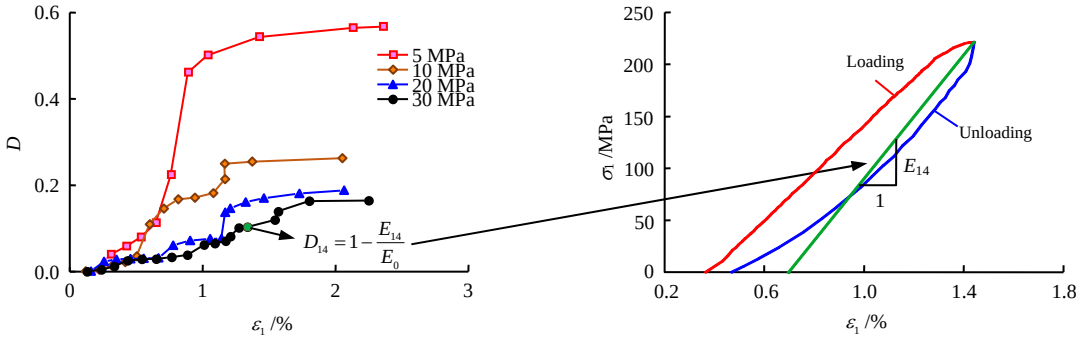


(a) Relationship curves of damage variable $D$ and axial strain $\varepsilon_1$ (b) Determination of the 14th cycle damage variable at 30 MPa

**Fig. 5 Relationships between damage variable and axial strain**

and the growth rate is increasing. When the strain is about 1.2%, the damage dissipation can produce a rapid surge process, which corresponds to the peak stress of the rock. Then the damage dissipation energy enters the linear phase, which corresponds to the residual stress stage of the rock. The main source of dissipated energy in this process is the friction of the fracture surface. Since the frictional energy and the slip distance approximately satisfy the linear law, the dissipated energy in this process is proportional to the axial strain.

Three stages can be roughly identified from Fig. 5, namely the slow development stage, the surge stage and the stable stage. When the rock enters the residual stress stage, the damage evolution gradually stops.

From the stress–strain relationship (Fig. 3), it can be found that under 5 MPa confining pressure, the slope of the unloading curve at the residual stress stage changes significantly as compared with that before peak, indicating that the loss of elastic modulus is greater. While under 30 MPa, the slope of the unloading curve at residual stress stage changes slightly as compared with that before peak, indicating that the loss of elastic modulus is smaller. Based on the damage variable definition method of elastic modulus, the greater the loss of elastic modulus, the greater the damage variable. The test results show that the damage variable eventually approaches a limit less than 1, and the larger the confining pressure, the smaller the limit value.

Considering the test results of damage dissipated energy and damage variables, we can draw a diagram of the relationship between damage dissipated energy and damage variables, as shown in Fig. 6. In the figure, the abscissa represents the damage variable, and the ordinate represents the damage dissipated energy. It can be seen from the figure that the dissipated energy shows a positive correlation law with the increase of the damage variable, and the growth rate of the dissipated energy is different under different confining pressures. A higher confining pressure gives a faster growth rate.

The damage dissipated energy–damage variable curve illustrates that a surge phenomenon eventually appear in development of dissipated energy, which is related to the characteristics of the residual stress stage. In the residual stress stage, due to the friction of the fracture surface continuously dissipating energy, at this time the elastic modulus approaches a constant, the damage variable no longer increases, showing the phenomenon that the damage variable does not change but the energy continues to be dissipated, so the curve shows an upward development trend.

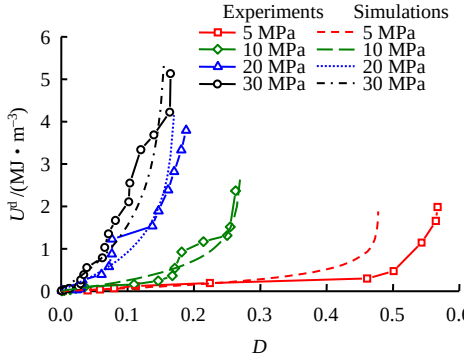


**Fig. 6 Relationships between damage dissipation energy and damage variable**

According to the definition of damage energy consumption rate, the energy consumed per unit damage in unit volume, the dimension of damage energy consumption rate $Y$ is determined as

$$\dim[Y]=\mathrm{ML}^{-1}\mathrm{T}^{-2} \tag{20}$$

where M, L, T are the dimension symbols of mass, length, and time, respectively.

It can be seen from the test results (Fig. 6) that the confining pressure and damage variables have a significant impact on the damage energy consumption rate. The greater the confining pressure, the greater the damage energy consumption rate. Additionally, the damage energy consumption rate approaches infinity when the damage variable approaches $D_{\max}$, thus the denominator adopts the form of ($D_{\max}-D$).The following model is constructed to describe the magnitude of the damage energy consumption rate:

$$Y=\frac{k\sigma_3+Y_0}{D_{\max}-D} \tag{21}$$

where $D_{\max}$ is the limit of damage variable, which denotes the limit value of the damage variable in the residual stress stage under a given confining pressure; $k$ is the influence coefficient of confining pressure on the damage energy consumption rate, which is a dim-

ensionless quantity; $Y_0$ is the damage energy consumption rate when the confining pressure is 0, and the dimension of energy consumption rate is $\dim[Y_0]=\mathrm{ML^{-1}T^{-2}}$, while the dimension of confining pressure is $\dim[\sigma_3]=\mathrm{ML^{-1}T^{-2}}$. In addition, since the damage variable is a dimensionless quantity, the dimensions of the left and right sides of Eq. (21) are the same.

First determine the expression of $D_{\max}$. Through the test results, the damage variable limits under the conditions of 5, 10, 20, and 30 MPa are: 0.567, 0.263, 0.188, and 0.165, respectively. For uniaxial compression conditions, since the rock cannot bear load in the post-peak stage, the elastic modulus is considered to be 0 at this time, so the damage variable is 1. The statistics of the above results are shown in Fig. 7. The test results are regressed and the exponential model is used, namely

$$D_{\max}=b_1\mathrm{e}^{b_2\sigma_3}+b_3 \tag{22}$$

where $b_1$, $b_2$ and $b_3$ are all empirical parameters.

The parameters $b_1$, $b_2$, $b_3$ are determined by fitting, and the expression of the limit of damage variable is obtained as

$$D_{\max}=0.84\mathrm{e}^{-0.2\sigma_3}+0.16 \tag{23}$$

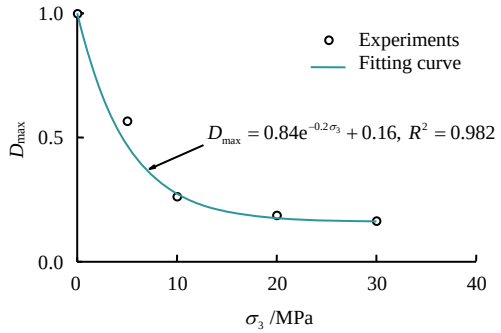


**Fig. 7 Relationship between damage variable limit and confining pressure**

After calculation, the goodness of fit is 0.982, indicating that the exponential model can more accurately represent the influence of the limit of the damage variable along with the confining pressure.

In order to further determine the parameters in the damage energy consumption rate *Y*, according to the definition of damage variable, the following formula is integrated using a numerical calculation method:

$$U^{\mathrm{d}}=\int Y\mathrm{d}D \tag{24}$$

After the relationship of $U^{\mathrm{d}}-D$ is obtained, the least square method is used to determine the best fitting parameters in the model. After fitting, the parameters $k=3.0$ J/(m$^3$·Pa), $Y_0=5$ MJ/m$^3$, and the goodness of fit is 0.934. The fitting result is presented as the solid line in Fig. 6, indicating that the fitting result can roughly reflect the relationship between the damage dissipated energy and the damage variable limit under different confining pressure conditions.

### 3.2 Plastic yield function and plastic potential function

The Mohr-Coulomb model (M-C model) is introduced to describe the strength of the rock, and the (shear) plastic yield function is [21–22]

$$f^{\mathrm{s}}=\sigma_1-\sigma_3N_\varphi-2c\sqrt{N_\varphi} \tag{25}$$

where *c* is the cohesion; $N_\varphi$ is related to the friction angle, and its expression is

$$N_\varphi=\frac{1+\sin\varphi}{1-\sin\varphi} \tag{26}$$

For rock-like materials, the direction of plastic flow is usually not along the normal direction of the loading surface. Therefore, the non-associated flow rule is adopted and the plastic potential function is assumed to be [21]

$$G^{\mathrm{s}}=\sigma_1-\sigma_3N_\psi \tag{27}$$

where $N_\psi$ is the material constant, which is related to the dilatancy angle $\psi$ of the material.

When the rock is in tension, its plastic yield function is

$$f^{\mathrm{t}}=-\sigma_3-\sigma_{\mathrm{t}} \tag{28}$$

where $\sigma_{\mathrm{t}}$ is the tensile strength. Since the compressive stress is assumed to be positive, there is a negative sign for $\sigma_3$ before it.

Under tension, the plastic potential function $G^{\mathrm{t}}$ adopts the associated flow rule:

$$G^{\mathrm{t}}=-\sigma_3 \tag{29}$$

## 4 Model validation

### 4.1 Calibration of model parameters

The parameters in the model involve three parts, namely: elastic part, damaged part and plastic part. The elastic part includes two parameters, namely the initial elastic modulus $E_0$ and Poisson's ratio $\mu$, which can be gained by the axial stress–strain curve and the axial strain–radial strain curve in the linear elastic stage of the loading process. The damage part only contains the parameters in the damage energy consumption rate *Y*, see section 3.1.

The plastic part parameters include cohesive force *c* and friction angle $\varphi$. First determine the initial yield stress, as shown in Fig. 8. The position where the stress–strain curve deviates from the fitting line of the linear stage is defined as the initial yield stress, as shown in the figure. Draw the initial yield stress Mohr's circle and the envelope to determine the cohesive force *c* and the friction angle $\varphi$, as shown in Fig. 9.

To further characterize the hardening–softening characteristics of the rock after yielding, the concept of equivalent plastic strain $\varepsilon^{\mathrm{ps}}$ is introduced, and its expression is

$$\varepsilon^{\mathrm{ps}}=\frac{1}{\sqrt{2}}\sqrt{\left(\varepsilon_1^{\mathrm{p}}-\varepsilon_{\mathrm{m}}^{\mathrm{p}}\right)^2+\left(\varepsilon_{\mathrm{m}}^{\mathrm{p}}\right)^2+\left(\varepsilon_3^{\mathrm{p}}-\varepsilon_{\mathrm{m}}^{\mathrm{p}}\right)^2} \tag{30}$$

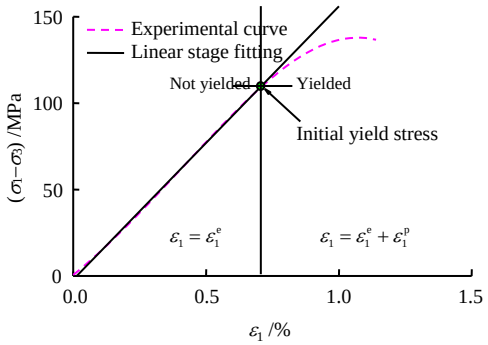


**Fig. 8 Determination of initial yield stress**

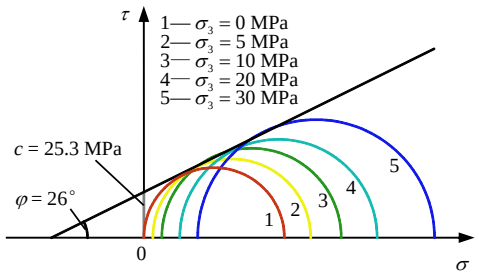


**Fig. 9 Determination of cohesion and friction angle**

where $\varepsilon_m^p$ is the plastic volumetric strain, and $\varepsilon_m^p = \left(\varepsilon_1^p+\varepsilon_3^p\right)/3$。

The relationship between the equivalent plastic strain and the cohesion and friction angle is plotted in Fig.10. Assuming that the cohesive force and friction angle of the rock are in a functional relationship with $\varepsilon^{ps}$, a line segment is used to approximate the smooth curve.

To determine the dilatancy angle, the relationship curves between axial strain $\varepsilon_1$ and volumetric strain $\varepsilon_v$ during the test are drawn first, as shown in Fig. 11. Then the dilatancy angle $\psi$ can be calculated by determining the included angle between the curve and *x*-axis in the shear expansion stage[23], and the calculation formula is as follows:

$$\psi = \arcsin\left(\frac{\tan\theta}{2+\tan\theta}\right) \tag{31}$$

Finally, $\theta_5$, $\theta_{10}$, $\theta_{20}$ and $\theta_{30}$ (where the subscript denotes the confining pressure) are respectively determined, and the corresponding dilatancy angles $\psi$ are obtained. By taking the average value for various confining pressure conditions, the dilatancy angle is calculated as 33.75°.

### 4.2 Model validation

To program the model in this article, C++ software is employed to build DLL (Dynamic Link Library) to realize the embedding of the model in FLAC$^{3D}$ software. FLAC$^{3D}$ is adopted to establish a cylindrical numerical simulation specimen with a total of 8000 elements and 7 980 nodes. As shown in Fig. 12, the model size, boundary conditions and loading conditions are consistent with the conventional indoor triaxial test.

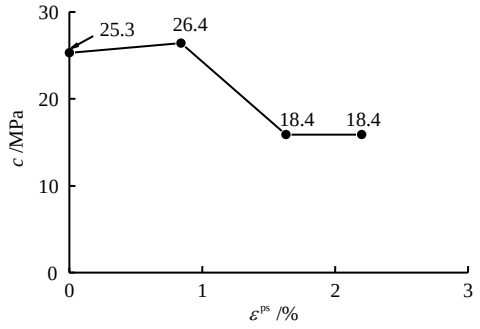


(a) Relationship between cohesion and equivalent plastic strain

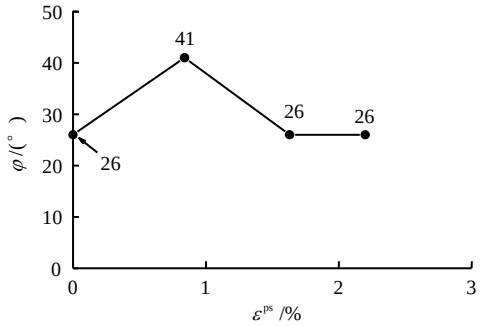


(b) Relationship between friction angle and equivalent plastic strain

**Fig. 10 Relationships of cohesion and friction angle with equivalent plastic strain**

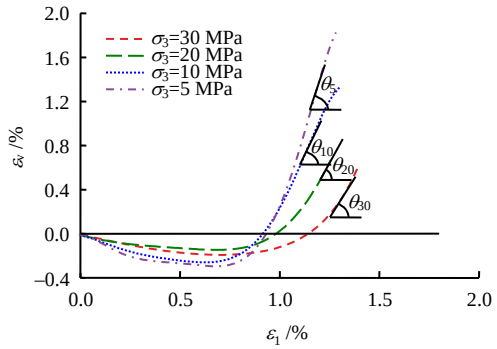


**Fig. 11 Relationships between volumetric strain and axial strain**

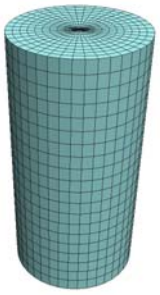

**Fig. 12 Numerical mesh model**

The model parameters consist of three parts: elastic part, with initial elastic modulus $E_0$ of 19.8 GPa, and Poisson's ratio $\mu$ of 0.24; plastic part, with dilatancy angle $\psi$ 33.75°, cohesion and friction angle as shown in Fig. 10; damage part, with influence coefficient $k$ of confining pressure of 3 J/(m$^3$·Pa), and initial damage energy consumption rate $Y_0$ of 5 MJ/m$^3$, and the

damage variable limit is shown in Fig. 7.

The comparison between the numerical simulations and the laboratory test results is illustrated in Fig.13, which gives the relationship between the axial strain and the radial strain.

From figure, it can be seen that the model reflects the strain hardening of the rock and the softening characteristics after the peak. And the model can describe the strain law of the rock in the third principal stress direction. Additionally, the peak strength increases as the confining pressure increases, which is obviously in line with the test results.

To ascertain the model's description of the characteristics of the damage dissipation energy, the relationship between the dissipation energy $U^{\mathrm{d}}$ and the axial strain $\varepsilon_1$ is plotted. Among them, the formula in the conventional three-axis numerical calculation process is [3]

$$U^{\mathrm{d}} = \sum_{\mathrm{step}=1}^{n} \left(\sigma_1 \Delta\varepsilon_1 + 2\sigma_3 \Delta\varepsilon_3\right) - \frac{1}{2E}\left[\sigma_1^2 + 2\sigma_3^2 - 2\mu\left(2\sigma_1\sigma_3 + \sigma_3^2\right)\right] \tag{32}$$

where the first item on the right side of the equal sign represents the work done by the outside on the unit rock, which is obtained by accumulating the calculation results of each step; $n$ represents the number of calculation steps; and the second term represents the elastic strain energy of the rock, and $E$ is the elastic modulus in the damaged state.

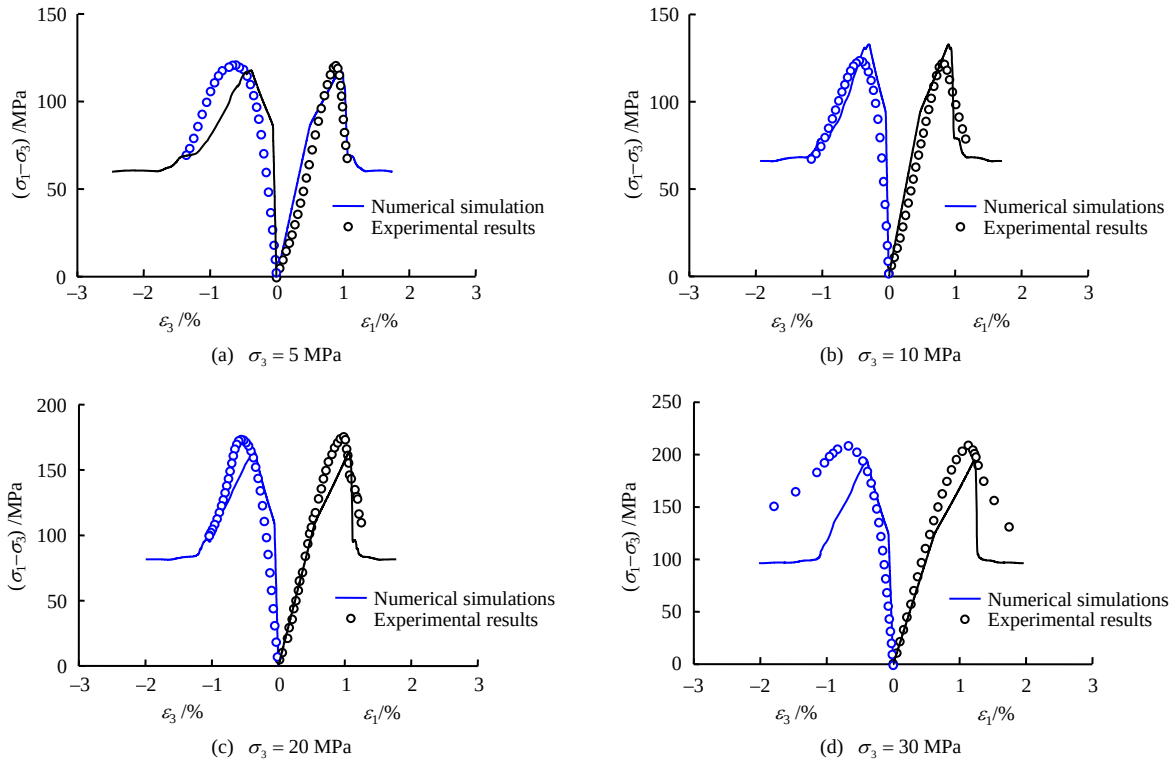


**Fig. 13 Comparison between numerical results and experimental results of rock stress–strain relationships**

Comparisons between the numerical results and the experimental results are made as in Fig. 14. It can be seen from the figure that the numerical results show three stages. In the strain hardening stage, the dissipated energy increases slowly; the dissipated energy increases sharply in the post-peak softening stage; and entering the residual stress stage, the dissipated energy increases linearly with the axial strain approximately. As a whole, the results by numerical calculation agree with those of experiment.

In order to further explore the model's description of the damage variable, the relationship between damage variable and axial strain in the numerical calculation process is drawn, as shown in Fig. 15. The test results show that the damage variable increases with the increase of axial strain, and the growth rate presents three stages of slow growth, rapid growth and stability (close to the limit of damage variable).

Numerical calculation results show that the model in this paper can describe the change law of rock damage variables more accurately.

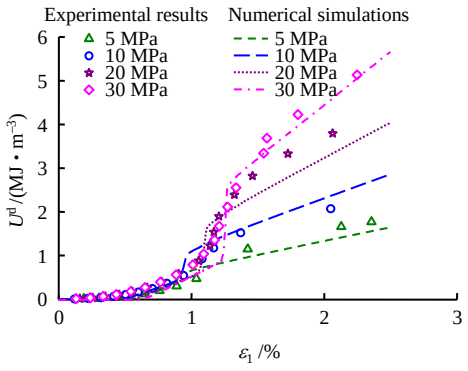


**Fig. 14 Relationships between dissipated energy and axial strain**

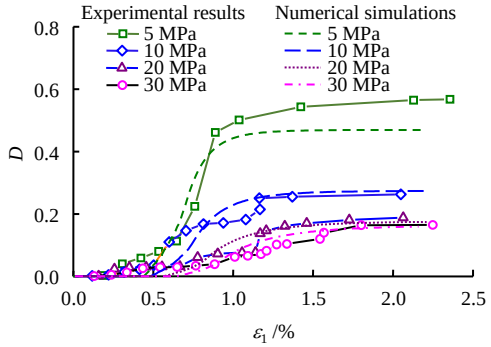


**Fig. 15 Experimental and numerical results of damage variable changing with axial strain**

## 5 Conclusion

This paper aims to use the damage energy consumption rate to solve the damage variables, and then establish the plastic-damage constitutive equation. The expression of the damage energy consumption rate was determined using the cyclic loading and unloading tests, and the model parameters were calibrated. Numerical calculation tests were carried out and compared with the laboratory tests. Some conclusions were drawn as follows:

(1) The damage dissipated energy slowly increases with the axial strain in the linear elastic stage, presenting an upward concave curve, and the growth rate is increasing. The growth rate reaches the maximum near the stress peak, and the damage dissipation energy is approximately linear with the axial strain in the residual stage after the peak.

(2) The damage variable definition method associated with the elastic modulus is adopted. On this basis, the test results show that the damage variable has a damage variable limit less than or equal to 1. With the increase of confining pressure, the limit of damage variable gradually decreases.

(3) Numerical calculation results show that the plastic-damage constitutive model proposed in this paper can describe the stress–strain relationship of rock under different confining pressures, the evolution laws of dissipated energy and damage of rock.

## References

[1] XIE He-ping, ZHOU Hong-wei, XUE Dong-jie, et al. Research and consideration on deep coal mining and critical mining depth[J]. Journal of China Coal Society, 2012, 37(4): 535–542.

[2] HAN Chao, PANG De-peng, LI De-jian. Analysis of energy evolution during the step loading and unloading creep experiments of sandstone[J]. Rock and Soil Mechanics, 2020, 41(4): 1179–1188.

[3] QIN Tao, DUAN Yan-wei, SUN Hong-ru, et al. Mechanical characteristics and energy dissipation characteristics of sandstone under triaxial stress conditions[J]. Journal of China Coal Society, 2020, 45(Suppl.1): 255–262.

[4] XU Guo-an, NIU Shuang-jian, JING Hong-wen, et al. Experimental study of energy features of sandstone under loading and unloading[J]. Rock and Soil Mechanics, 2011, 32(12): 3611–3617.

[5] LI Zi-yun, WU Guang, HUANG Tian-zhu, et al. Variation of energy and criteria for strength failure of shale under traixial cyclic loading[J]. Chinese Journal of Rock Mechanics and Engineering, 2018, 37(3): 662–670.

[6] ZHANG Zhi-zhen, GAO Feng. Experimental investigation on energy evolution characteristics of coal, sandstone and granite during loading process[J]. Journal of China University of Mining & Technology, 2015, 44(3): 416–422.

[7] XIE He-ping, PENG Rui-dong, JU Yang. Energy dissipation of rock deformation and fracture[J]. Chinese Journal of Rock Mechanics and Engineering, 2004, 23(21): 3565–3570.

[8] XIE He-ping, JU Yang, LI Li-yun, et al. Energy mechanism of deformation and failure of rock masses[J]. Chinese Journal of Rock Mechanics and Engineering, 2008, 27(9): 1729–1740.

[9] JIANG Jing-dong, CHEN Sheng-shui, XU Jie, et al. Mechanical properties and energy characteristics of mudstone under different containing moisture states[J]. Journal of China Coal Society, 2018, 43(8): 2217–2224.

[10] YANG Sheng-qi, XU Wei-ya, SU Cheng-dong. Study on the deformation failure and energy properties of marble specimen under triaxial compression[J]. Engineering Mechanics, 2007, 24(1): 136–142.

[11] CONG Yu, WANG Zai-quan, ZHENG Ying-ren, et al. Energy evolution principle of fracture propagation of marble with different unloading stress paths[J]. Journal of Central South University (Science and Technology), 2016, 47(9): 3140–3147.

[12] LI Li-yun, XIE He-ping, JU Yang, et al. Experimental investigation of releasable energy and dissipative energy within rock[J]. Engineering Mechanics, 2011, 28(3): 35–40.

[13] ZHAO Yong-chuan, LIU Hong-lei, YANG Tian-hong, et al. Effect of mesozoic sandstone meso structure on strength and energy dissipation characteristic[J]. Journal of China Coal Society, 2017, 42(2): 452–459.

[14] QIAO L, CHEN L, DASGUPTA G, et al. Surface characterization and frictional energy dissipation characteristics of deep granite under high stress

conditions[J]. Rock Mechanics and Rock Engineering, 2019, 52(5): 1577−1589.

[15] YIN Guang-zhi, MA Bo, LIU Chao, et al. Effect of loading and unloading rates on mechanical properties and energy characteristics of sandstone under true triaxial stress[J]. Journal of China Coal Society, 2019, 44(2): 454−462.

[16] PENG R D, JU Y, WANG J G, et al. Energy dissipation and release during coal failure under conventional triaxial compression[J]. Rock Mechanics and Rock Engineering, 2015, 48(2): 509−526.

[17] HE M, HUANG B, ZHU C, et al. Energy dissipation-based method for fatigue life prediction of rock salt[J]. Rock Mechanics and Rock Engineering, 2018, 51(5): 1447−1455.

[18] NING J, WANG J, JIANG J, et al. Estimation of crack initiation and propagation thresholds of confined brittle coal specimens based on energy dissipation theory[J]. Rock Mechanics and Rock Engineering, 2018, 51(1): 119−134.

[19] LIU X S, NING J G, TAN Y L, et al. Damage constitutive model based on energy dissipation for intact rock subjected to cyclic loading[J]. International Journal of Rock Mechanics and Mining Sciences, 2016, 85: 27−32.

[20] KUPFER H K, HILSDORF H, RUSCH H. Behavior of concrete under biaxial stresses[J]. ACI Journal Proceedings, 1969, 656−666.

[21] LIU Yang, YANG Gang, WANG Jun-xiang, et al. Mohr-Coulomb elastoplastic damage constitutive model of rock and implicit return mapping algorithm in principal stress space[J]. Rock and Soil Mechanics, 2017(Suppl.1): 424−434.

[22] MA Qiu-feng, QIN Yue-ping, ZHOU Tian-bai, et al. Mechanical properties and constitutive model of porous rock under loading and unloading[J]. Rock and Soil Mechanics, 2019, 40(7): 2673−2685.

[23] VERMEER P A, BORST R D. Non-associated plasticity for soils, concrete and rock[J]. Heron, 1998, 29(3): 1−64.